Computers and Concrete, *Vol. 34, No. 5 (2024) 547-560*
https://doi.org/10.12989/cac.2024.34.5.547

Parametric study on the damage to concrete matrices by induction heating of its reinforcement

Aimar Orbe*[1], Roque Borinaga-Treviño[2], Ignacio Crespo[3] and Olatz Oyarzabal[2]

[1]*Construction Engineering Area, Department of Mechanical Engineering, Engineering Faculty of Bilbao, University of the Basque Country (UPV/EHU), Plaza Ingeniero Torres Quevedo 1, 48013, Bilbao, Spain*
[2]*Mechanics of Continuous Media and Theory of Structures Area, Department of Mechanical Engineering, Engineering Faculty of Bilbao, University of the Basque Country (UPV/EHU), Plaza Ingeniero Torres Quevedo 1, 48013, Bilbao, Spain*
[3]*Industry and Transport Department, TECNALIA Research & Innovation, Basque Research and Technology Alliance (BRTA), Paseo Mikeletegi 2, 20009, Donostia-San Sebastian, Spain*

(*Received December 11, 2021, Revised December 21, 2021, Accepted March 13, 2024*)

Abstract. Concrete structures may be subjected to repair or local dismantling due to changes in the activity or in case of their damage. Current demolition techniques, besides the required time frame for the renewal, involve remarkable affections due to noise, vibration and dust. This research presents a method to carry out such procedures selectively and efficiently, avoiding noticeable affections on the environment and other users. In addition, it could ease the segregation of the construction materials for better recycling. The study analyses the influence of the position and diameter of the reinforcement, the frequency of the applied magnetic field, the thermal conductivity and the specific heat capacity of the surrounding cementitious matrix and the convection and radiation phenomena on the induction heating process. Depending on the setup, high temperatures (above 700 °C) can be achieved in less than 90 s. However, the frequency and the reinforcement position are the most influential parameters, showing a heating rate up to a 300% faster when increasing the frequency 4 times (from 12 kHz to 48 kHz) and a difference up to 250% in the maximum temperature achieved between rebars aligned and misaligned with the magnetic field. A regression analysis performed on the data obtained provides a prediction model that properly fits (R^2=0.979) the expected heating according to the variable parameters. Finally, a real scale column case is simulated and observed that closed stirrups can increase the heating above 1000 °C in just 60 s and induce cracking of the matrix.

Keywords: concrete cracking; concrete reinforcement; Joule effect; magnetic permeability; temperature

1. Introduction

Electromagnetic induction is widely applied in automotive industry, forging, tube manufacturing, etc. Diverse metals can be melted, welded, annealed or hardened through its use as explained in Davies (1990). It differs from direct resistance heating, due to the absence of contact between the equipment used and the part to be heated. Besides, it is much more effective since it does not heat the surrounding air between the inductor and the part to be heated. Therefore, the workpiece is directly heated, reducing energy losses. However, electromagnetic techniques are not commonly considered in the construction sector.

Construction is a influencing sector on the Gross Domestic Product (GDP) when comparing developed countries. Each percentage increase in the former leads to almost double the increase in the latter (Qabaja and Tenekeci 2023). Concrete, and such cementitious materials, are the most widely used construction materials worldwide, covering up to 47% of the Domestic Material Consumption (DMC) in the EU-28 zone (European Environment Agency 2020), and the rise or fall of this activity can be measured through an analysis of concrete consumption over time. However, its high consumption is not balanced with widely extended and implemented processes that allow its selective demolition or the recycling of its components into quality raw materials (Di Maria *et al.* 2020), with landfill still prevailing in up to 35% of the Construction and Demolition Waste (CDW) (Kabirifar *et al.* 2020). The European Waste Framework Directive 2008/98/EC (European Commission 2018) established a target of 70% of CDW recycled by 2020. So far, few countries have surpassed the target and the average recycling rate is about 50% (Zhang *et al.* 2023, Fufa *et al.* 2023). Until recent times, as in other industries or sectors, the scope of the construction process was centred on a simplistic concept that ended with the delivery of the final product. In this situation, the demolition or reuse of latent resources available in the structures or buildings was not contemplated (Luu *et al.* 2021). Besides the inadequate initial cradle-to-gate approach and even the intermediate cradle-to grave that, even considering issues related to rehabilitation like in Moncaster and Symons (2013), did not consider the potentiality of the by-products originated by demolition, currently the cradle-to cradle approach is the most complete (Silvestre *et al.* 2013, 2014, Lei *et al.* 2021, Lynch 2022). The reuse of construction and demolition

*Corresponding author, Ph.D.
E-mail: aimar.orbe@ehu.eus

ISSN: 1598-8198 (Print), 1598-818X (Online)

waste (CDW) is fundamental to promote the Circular Economy (Hondroyiannis *et al.* 2024), so necessary to boost the level of sustainability of the structures according to the new European framework to assess and report on the sustainability of buildings (De Wolf *et al.* 2023).

Although among the construction materials, the concrete presents the best behaviour at high temperatures, eventually its constituent components degrade. And so do the rebar reinforcement held inside the concrete, which can be subjected to corrosion processes and damage the surrounding cementitious matrix. While for temperatures below 100 ºC, the phenomena of dehydration of the cement paste and the expulsion of water vapour are the main reactions that occur, from this value and up to approximately 500 ºC, crystalline transformations are chained in the aggregates and cement paste according to RILEM Technical Committee 227 (2019b). As an example, the decomposition of calcium carbonate occurs from 400 ºC on RILEM Technical Committee 227 (2019a). Consequently, the tensile strength of the cementitious matrix is proportionally reduced. Above 1200 ºC, the concrete components melt, presenting a liquid state. Several studies deal with the consequences of high temperatures in the concrete, such as, fire hazards (Kim and Kwak 2017, Li *et al.* 2019), spalling (Ozbolt *et al.* 2008) and the influence of recycled aggregates (Liang *et al.* 2017, 2018) or foamed concrete (Canbaz *et al.* 2019).

Previous research have analysed the use of electromagnetic fields, such as microwaves, to segregate the cement paste from the aggregates and obtain recycled raw materials of adequate quality (Menard *et al.* 2013). Research focused on curing concrete (Ahn *et al.* 2021) or healing concrete asphalt materials through electromagnetic methods, microwave or induction, are more usual (García *et al.* 2013, Norambuena-Contreras *et al.* 2016). Aligned with the findings of this research, it could be proved feasible to consider the application of induction heating to activate self-healing capsules mixed within the cementitious matrix, increasing the life cycle of the structures and providing more sustainable structures. Likewise, other studies focus their efforts to assess its feasibility as a non-destructive test method. Inductive methods have been successfully applied to assess the fibre orientation and amount within steel fibre reinforced concretes as proved in Torrents *et al.* (2012), Ferrara *et al.* (2012), Orbe *et al.* (2014). Induction heating and infrared thermography have also been adapted for the detection of the corrosion of the reinforcement embedded in concrete successfully in the studies of Kobayashi and Banthia (2011), Zhang *et al.* (2017), Sannikov *et al.* (2018), Liu *et al.* (2018). In that case, as the aim was not to further deteriorate the constituent materials of the section, the temperatures reached were kept in a reduced range, compared to those that are intended to be achieved in the present study. Nonetheless, currently the target of various studies (Akbarnezhad and Ong 2011, Ong and Akbarnezhad 2015, Lim *et al.* 2017, Borinaga-Treviño *et al.* 2019) resides on shedding light on their potential as demolition techniques. Although, considering the complete demolition by means of the aforementioned techniques may be energetically costly, this approach is interesting for the more localised separation of materials that allow a more affordable rehabilitation of structures and a more effective recycling of materials as described in Lim and Kim (2017). The approaches may be various and diverse, from the detection of pathologies, the demolition of structures or the increase in performance of the RCD through the recycling of their aggregates. The present study, however, proposes a possible way to apply these concepts to structures that, presenting injuries, such as the corrosion of reinforcements, are not intended to be demolished, but to be repaired. Therefore, it is essential to remove the material covering the reinforcements, which is generally carried out by chopping processes that generate notable conditions in the form of noise, vibrations, dust, etc., in addition to the consumption of material resources, human and, above all, time. An electromagnetic technique could, in a matter of a few minutes, allow its removal without causing any of the aforementioned conditions. There already are studies that analyse the degradation of the bonding between rebar and concrete at high temperatures (Yan *et al.* 2019, Lim and Lee 2021c).

Although there are analytical solutions found in the literature for determining the temperature increment of a workpiece, they are suitable only for simple geometries as those shown in Luozzo *et al.* (2012), Kennedy *et al.* (2012), Jankowski *et al.* (2016). The following section (Section 2) presents the materials, procedures and parameters to be analysed. The main parameters involved in the heating process are, hence, analysed through real tests and computational simulations while their influence in the overall performance is assessed. The third section (Section 3) plots the heating rate of all the tests and simulations carried out providing a straightforward view of the most influential parameters. Besides, a regression analysis is carried out, leading to a satisfactory prediction of the temperature increment. Next (Section 4), the study approaches the effect on larger elements, such as columns, going beyond laboratory-scale specimens. The final Section (Section 5) summarises all the findings and provides guidance for further research on this topic.

This research aims to provide a method to provoke and predict the degradation of the bonding between rebar and concrete at high temperatures, not due to fire hazards, but in a local and controlled way. This goal will lead to establishing an emerging line of research in the field of construction and, especially, with regard to the technology of reinforced concrete.

2. Materials and methods

As a first stage an experimental campaign has been carried out providing real data that will be necessary for the validation of the simulation model. The following stage, is focused on analysing the main parameters involved which can influence the induction heating performance of steel reinforced cementitious matrices.

The simulation involves solving Maxwell's equations (see Eq. (1)). According to Gauss's laws, a null divergence of the magnetic field (B) is assumed, while the divergence

(a) Real case study

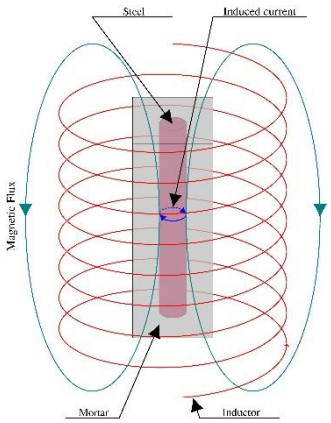

(b) Magnetic fields and induced current

Fig. 1 Helix inductor

of the electric field E depends on the volume charge density (ρ) and the permittivity of free space (ε_0). In agreement with Ampere's law, the alternate electric current density (J) flowing through a sinusoidal coil leads to an alternate magnetic field (B) inside it, being μ_0 the permeability of free space. Placing a ferromagnetic and electrically conductive material, as the steel reinforcement, within the magnetic field creates an opposing electromotive force (ε) due to the induced current or "Eddy currents" in accordance with Faraday's and Lenz's laws and depicted in Fig. 1(b).

$$\begin{aligned} \nabla \cdot \mathrm{B} &= 0 \\ \nabla \cdot E &= \frac{\rho}{\varepsilon_0} \\ \nabla \times B &= \mu_0 \cdot J \\ \varepsilon(V) &= -\frac{d\Phi_B}{dt} \end{aligned} \tag{1}$$

There are two phenomena that increase the temperature in the steel rebar, namely, the Eddy currents heating and the Hysteretic heating. On the one hand, the former is caused by the resistivity losses (I^2R) of the induced currents flowing along the surface of the rebar, known also as Joule effect. On the other hand, the latter is derived from the changing of the magnetic polarity of the rebar due to the alternating magnetic field. Up to the Curie temperature both phenomena are simultaneous, while only Eddy current heating remains henceforth (Lim and Lee 2021a).

The heat transfer to the cementititous matrix depends on the thermal conductivity and specific heat capacity of both materials in contact, mortar or concrete and steel, that condition the heat exchange between them. Finally, convection and emissivity parameters influence the cooling rate of the mortar surface in contact with the air.

2.1 Experimental stage

Although the proposed method would be appropriate for any cementitious matrix, be it mortar or concrete, since this approach is based on currently commercially available inductor shapes, laboratory scale mortar specimens have been cast. The batch of the experimental stage comprises the mix of cement type II, limestone crushed sand, water up to a 0.5 w/c ratio and 1.5% of weight of cement as polycarboxylate ether based superplasticizer, as described in Table 1.

Table 1 Mix design

Cement (kg/m^3)	Sans (kg/m^3)	Water (L/m^3)	Admixture (L/m^3)
450	1700	225	6.75

Three specimens, 40×40×160 mm in size, were cast with a 150 mm long corrugated steel rebar centred inside. Each of the rebars has attached thermocouples to measure the temperature increment along the test. Fig. 1 shows the power supply and inductor used during the experimental stage (Fig. 1(a)) and an illustration of the generated magnetic fields and eddy currents (Fig. 1(b)).

2.2 Parametric study

Initially, and replicating the real test performed, mortar specimens with rebars embedded have been modelled. This first step has allowed to validate the simulation model against real tests.

Since on site reality can differ from controlled laboratory environments due to several causes, multiple simulations have been analysed varying individual parameters. On the one hand and although physical properties of steel are stable enough, cementitious matrices are heterogeneous and porous materials that depending on their porosity and moisture content can present variable behaviours. On the other hand, and due to the difficulty to modify some of them in real tests, some other parameters have been adopted through simulations. Firstly, the mesh sensitivity has been studied, generating finer and coarser meshed models. These have been compared with the experimental results in order to check which would be an adequate element amount for matching the results reasonably. Since the distance from the inductor and the alignment according to the magnetic field alters the response of the material, various positions of the specimen have been controlled, arranging them vertically centred, off-centred and even horizontally. The working frequency of the used induction equipment is fixed to 24 kHz, but the simulations have allowed to determine the behaviour of the

Table 2 Considered variables

Diameter Φ (mm)	Position	Frequency f (Hz)	Thermal Conductivity* λ (W/m·K)	Specific Heat Capacity* C_p (J/kg·K)	Convection h	Emissivity ε	Mesh (Element #)
8	vertical centred	12000	1	500	1	0.3	≈255000
10	vertical lateral	24000	1.5	750	10	0.8	≈800000
12	horizontal centred	48000	2	1000	100	0.95	≈1080000

*The reference case does not consider a constant thermal conductivity nor a constant specific heat capacity; The values are adopted according to RILEM Technical Committee 227 (2019a).

specimen for a wider range of frequencies (f). In addition, the influence of inherent parameters of the mortar matrix, such as, the thermal conductivity (λ) and specific heat capacity (c_p), have also been checked. However, it must be remarked that the reference model does not consider constant values for the latter parameters, assuming the ones established in RILEM Technical Committee 227 (2019a). Finally, diverse boundary conditions have been tested, from natural to forced convection (h) and low and high radiation emissivities (ε). All these values are summarised in Table 2. Each column presents the adopted values for each parameter. The values in the reference case are highlighted in bold.

The fine simulation model considers the real shape of the rebar including the surface corrugation and a hollow tube as inductor. It comprises 1080 k finite tetrahedral elements approximately and takes 46 hours and 27 minutes to simulate 240 seconds of real time (32 GB, 2 Intel® Xeon® E5-2637 v4® Processors, 3.50 GHz). The medium model simplifies the rebar geometry, modelling it as a plain cylinder, generating up to 800k elements and reducing the computation time to 19 hours and 2 minutes. Finally a, third, coarser model is established, neglecting the refrigeration conduct within the inductor and, therefore, expanding the discretization around its path. The mesh is formed by almost 255 k elements, lasting 7 hours and 23 minutes of computational time. All of the models comprise a viscous layer of up to 8 layers within a 0.3 mm thickness from the surface.

The medium models requires almost 59% less computation time and the temperatures are quite similar to those measured for the fine model. Moreover, both show a remarkable similarity with the experimental results. The coarse model demand is more reduced (up to 84%) but although it reaches the same final temperature, it does not track the ascending branch properly. Since the steel acquires the same final temperature in all the simulations and no other parameter has been modified, the temperature gradient through the cementitious matrix is identical. Hereinafter, all the simulations are carried out considering the medium model as the reference case. The successive simulations runs up to 90 s, when the temperature is limited by an upper asymptote as a result of its proximity to the Curie point.

All the simulations consider the same geometry and similar meshing, except the ones regarding the diameter sensitivity and the frequency sensitivity. It is evident that the former requires a different geometry and, therefore, an adapted mesh; coarser as the diameter increases. The latter

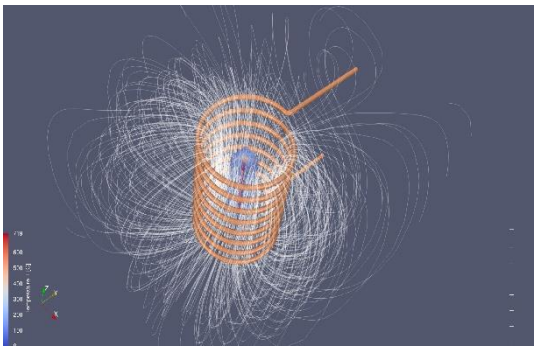

(a) Test simulation

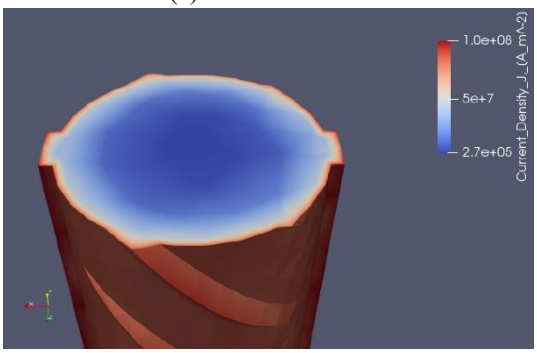

(b) Skin effect in the cross section of the rebar

Fig. 2 Induction test

requires modifying the viscous layer located in the surface of the rebar. Since the current induced due to the magnetic field flows very shallow, a very fine mesh is necessary along its surface (see Fig. 2(b)) (Lim and Lee 2021b). The depth of penetration where the skin effect is noticeable depends on the frequency (f), the resistivity (ρ) and the permeability (μ) of the steel and is determined according to Eq. (2). This thickness corresponds to the layer where approximately the 63% of the current density is induced. The frequencies selected in the present study can be considered high, since the goal is focused on damaging the interface between concrete and steel in the shortest time possible. The higher the frequencies applied, the lower would be the penetration depth. Hence, the target of the heating process is the steel surface, regardless of the core of the rebar.

$$\delta = \sqrt{\frac{2 \cdot \rho}{\mu \cdot \omega}} \tag{2}$$

The parameters of the steel involved in the induction heating process are not constants through the whole

(a) Cracking on tested specimen

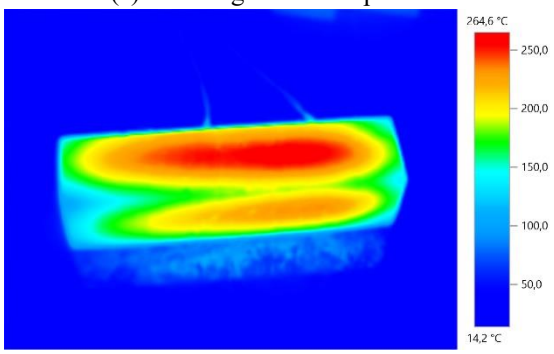

(b) Surface temperature on tested specimen

Fig. 3 Thermographic image of tested specimen

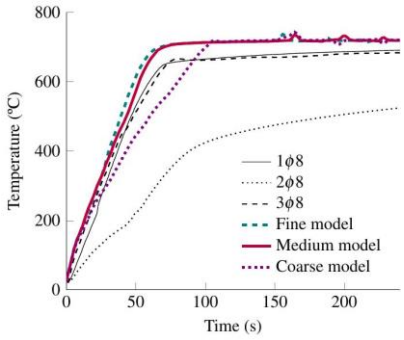

(a) Temperature increment on the steel

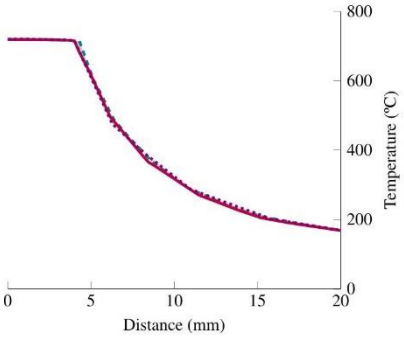

(b) Temperature gradient on the concrete

Fig. 4 Mesh influence in the temperature

process. Mainly, the relative permeability (μ_r) is the one that can alter the behaviour in a greater extent. Instead of considering the variability of magnetic flux density (B) according to the magnetic field intensity (H), due to its high computational cost, a temperature dependence approach is adopted according to previous studies of Nemkov and Goldstein (2017). The magnetic permeability considered in each time step is corrected through Eq. (3), where μ_r stands for the initial value of the permeability, T for the temperature of the current time step, T_c for the Curie temperature and β for a parameter that defines the convex shape of such correction.

$$\mu(T) = 1 + (\mu_r - 1) \cdot \left(1 - \left(\frac{T}{T_c}\right)^{\beta}\right) \tag{3}$$

The thorough study of all this parameters will allow to scale the model to real applications in any construction field. To this end, a regression analysis is performed with all the recorded data. Since the heating process presents an ascending branch and an upper asymptote, a logistic function is considered the best option to fit the data. Logistic functions are widely used to analyse growth trends in multidisciplinary topics such as biology, social sciences, chemistry and, even, concrete structures as in Wang *et al.* (2020).

3. Results

The process of heating the rebar inside the cementitious matrix lead to an evident cracking along the length of the steel reinforcement due to a thermal shock. Fig. 3(a) shows the crack pattern of one of the tested specimens. The noticeable damage of the mortar is caused within the first 90 s of the test, where an upper asymptote of the temperature increment is located.

In all the cases, the maximum temperature in the rebar through time and the final maximum and minimum temperature gradients from the centre of the specimen to the mortar surface have been assessed. The following subsections show the results for each of the modified parameters.

3.1 Mesh sensitivity

First of all, a mesh sensitivity study has been performed in order to assure that the results are accurate and, in addition, the computational cost does not escalate exponentially. The obtained values are validated against real induction test (see Subsection 2.1) performed on specimens that have been replicated through the simulations. The maximum temperatures achieved in the rebar through time and the final maximum and minimum temperature gradients from the centre of the specimen to the mortar surface have been assessed and shown in Fig. 4.

The experimental values show some differences, due to the inherent heterogeneity of the cementitious matrices. The difficulty of measuring locally such parameters as thermal conductivity and specific heat capacity, or even others as pore location and moisture in such pores, lead to a slightly dissimilar behaviour in each specimen. Besides, the specimens tend to crack due to thermal shock when heating suddenly the steel reinforcement. The complexity of the crack patterns also lead to differences in the mentioned parameters and therefore, to different results. However, specimen 2*Φ*8 does not achieve the expected temperature

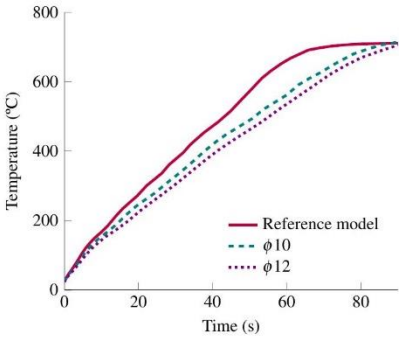

(a) Temperature increment on the steel

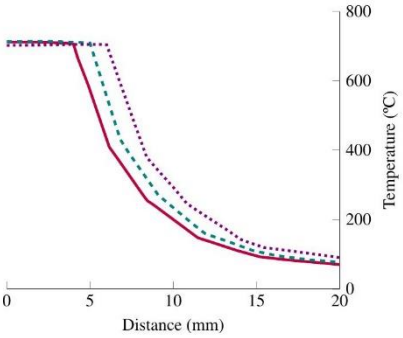

(b) Temperature gradient on the concrete

Fig. 5 Diameter influence in the temperature

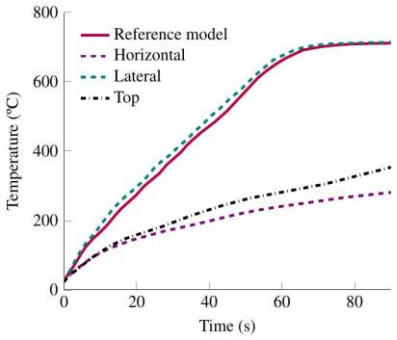

(a) Temperature increment on the steel

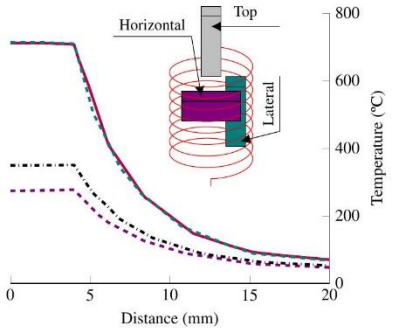

(b) Temperature gradient on the concrete

Fig. 6 Position influence in the temperature

and must be discarded, since the thermocouples were detached from the reinforcement during the compaction process on a shocking table. Therefore they do not measure the temperature in the proper location, surface of the rebar, but some place within the cementitious matrix, between the rebar and the mortar surface. Nevertheless, the rest of the results lay in a similar range of temperature values, which accuracy is enough for the sought purpose.

3.2 Diameter sensitivity

As it can be observed in Fig. 5, the higher the rebar diameter, the slower is the temperature increment. The target volume of steel affected by eddy currents increases and therefore, the heating rate reduces proportionally. Although the reference model reaches the upper asymptote within 70 s, the higher rebar diameters approach it in just 90 s, still fast enough. Regarding the heat transfer to the cementitious matrix, being the rebar diameter greater, its influence is noticeable in a larger proportion. However, surface temperatures only report negligible differences.

3.3 Position sensitivity

As depicted in Fig. 1(a), the magnetic flux is higher inside the inductor. Any attempt to displace the specimen will cause a remarkable drop in the heating rate. The lateral position remains within the coupling of the fields generated in each side of the coil. Positioning the specimen outside the inductor, causes a low effect since only the magnetic field created in the upper turns induces any current in the lower part of the specimen. Moreover, the orientation of the rebar plays a key role since the opposing *emf* weakens.

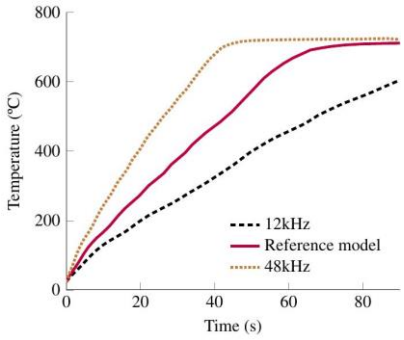

(a) Temperature increment on the steel

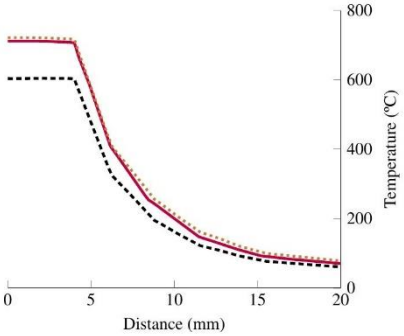

(b) Temperature gradient on the concrete

Fig. 7 Frequency influence in the temperature

Therefore, locating the specimen horizontally proves to be less effective (see Fig. 6).

3.4 Frequency sensitivity

Frequency is the main dominant parameter on the

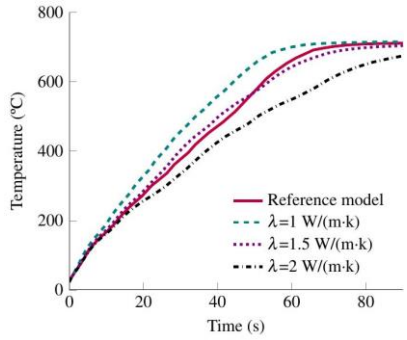

(a) Temperature increment on the steel

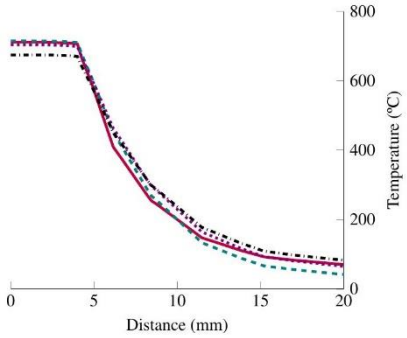

(b) Temperature gradient on the concrete

Fig. 8 Thermal conductivity influence in the temperature

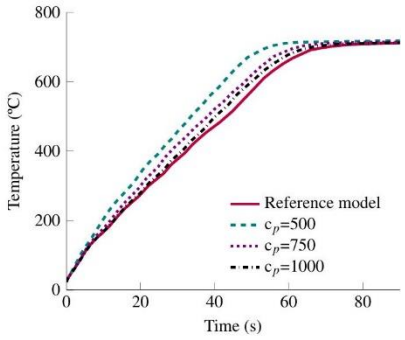

(a) Temperature increment on the steel

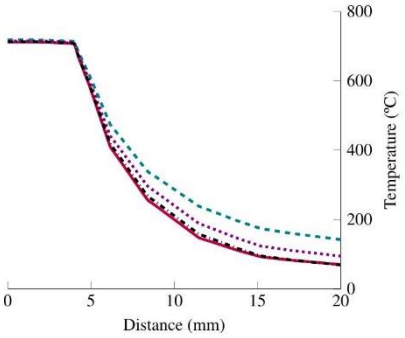

(b) Temperature gradient on the concrete

Fig. 9 Specific heat capacity influence in the temperature

heating rate of the ascending branch. As shown in Fig. 7, both, the highest frequency model and the reference model reach maximum temperature after 90 s, while the 12 kHz simulation achieves a 16% lower temperature value. Eventually all the specimens reach the upper asymptote, but depending on the frequency the maximum temperature can be achieved in a shorter time. However, the benefit of increasing the work frequency is limited, since the increment of heating rate is gradually reduced as the frequency increases.

3.5 Thermal conductivity sensitivity

Although the reference case considers variable thermal conductivity and specific heat capacity values, different cases have been analysed in order to assess the influence of such parameters in the overall performance of the established method. As can be observed in Fig. 8, the lower the thermal conductivity of the cementitious matrix, the faster the maximum temperature is achieved in the rebar. It is evident that the reduction of the heat transfer between both bodies benefits the heating process of the steel.

In the simulated time frame, the steel achieves similar temperatures in all the cases. Therefore, starting from a comparable value, the temperature in the mortar surface depends only in the adopted thermal conductivity value. Evidently, the lower the thermal conductivity, the lower the heat transfer through the mortar matrix and, hence, the lower the temperature at the surface. Although the temperature differences in the steel over time are relatively less significant than those obtained within the mortar surface (6.2% vs. 41%, respectively), in absolute values the differences are more noticeable (45 °C vs 29 °C, respectively).

The variable thermal conductivity of the reference model is initialized with a value of λ=2 W/(m·K) and gradually reduced up to λ=0.8 W/(m·K) for the maximum temperature. The behaviour, as expected, lies within the range of the rest of the simulations.

3.6 Specific heat capacity sensitivity

Specific heat capacity shows a similar trend as the one mentioned in the previous subsection (see Subsection 3.5). The concrete matrix does not require much power to be heated in case of the lowest c_p value. Therefore, the heating rate of the rebar is the highest among the simulations. Equally, the temperatures achieved in the mortar surface are the highest for this case.

Although the differences in the temperature increment of the steel (see Fig. 9(a)) are less remarkable than the ones related to the thermal conductivity, the variations in the mortar surface are noteworthy, up to 103% of the reference temperature.

The reference model considers a variable specific heat capacity for the cementitious matrix, being roughly c_p=1 kJ/kg·K except near the boiling temperature of the water. The evaporation of the moisture contained in the pores of the matrix, lead to a short peak of c_p=2 kJ/kg·K. As expected, the results are rather identical to those obtained for the highest specific heat capacity.

3.7 Convection and radiation heat transfer sensitivities

Convective heat transfer is assessed for multiple

Table 3 Fitting parameters

Case	*a*	*b*	*c*	c_p (J/kg·K)	λ (W/m·K)	ε (---)	*h* (---)	*f* (kHz)	Position	Φ
Reference	721.31	0.074	29.13	Var.	Var.	0.8	10	24	Vert. cent.	8
Φ10	716.10	0.061	35.48	Var.	Var.	0.8	10	24	Vert. cent.	10
Φ12	707.05	0.060	36.96	Var.	Var.	0.8	10	24	Vert. cent.	12
f12	605.99	0.058	37.23	Var.	Var.	0.8	10	12	Vert. cent.	8
f48	722.12	0.118	17.85	Var.	Var.	0.8	10	48	Vert. cent.	8

scenarios, natural, medium and forced. However the differences among all the cases are negligible. The surface area/volume ratio is not large enough to show noticeable differences. Although there are differences of up to 14% on the surface temperature, it can be argued that induction heating remains effective for indoor (factory) and outdoor (on site) applications, regarding the convection factor adopted. The temperatures within the matrix are still high enough to provoke the thermal shock and evaporate the moisture within the vacuolar pores to damage the mortar through their incremental pressure.

Similar to what has been stated for the convection sensitivity, emissivity neither is an influencing factor. The differences due to this factor do not exceed 2%. After 90 s of heating, the temperatures achieved in the mortar surface do not exceed 100 °C. Such temperatures are not high enough to exchange heat as thermal radiation. Therefore, there is not need for surface treatments, e.g. polish, in order to reduce the emissivity of the mortar. In order to avoid superfluous figures, the corresponding plots of these two parameters are not included in the manuscript.

3.8 Regression analysis

As aforementioned, the present subsection aims to define the parameters of a logistic function that could predict the heating process. The proposed equation (see Eq. (4)), considers several variables which define its shape. It is a simple approximation that fits adequately the given data over time, *t*, specially the abrupt slope change when reaching the upper asymptote. It is a continuously differentiable equation through all the studied domain. Its unique drawback is that it does not provide information of the initial stage up to 100 °C. However, being the main goal focused in remarkably higher temperatures, it is reasonable to discard those values. Among the variables, *a* stands for the maximum temperature to reach, *b* alters its characteristic curve shape modifying the growth rate and *c* establishes the abscissa coordinate of the inflexion point.

As previously observed, frequency and rebar diameter are notably the main parameters influencing the heating behaviour. Therefore, this subsection will summarise the multivariate linear regression conducted to predict the value of the parameters required in the proposed model from the applied frequency and the embedded rebar diameters.

Boundary conditions such as convection and emissivity have little effect on the maximum temperature reached on the steel rebar. These parameters determine the heat transfer between the mortar surface and the surrounding air. Accordingly, the significances obtained are low, even for the mortar surface temperature where they might play a key role.

Thermal conductivity and specific heat capacity however, alter the response on both cases since they imply diverse heat transfer amounts between rebar and matrix. However, since the reference model does not consider a constant value for these parameters, they are not considered within this regression model. The authors assumed that the values adopted in the Eurocode 2 (EN 1992-1-2, 2004) do cover correctly the common cases.

$$T(°C) = \frac{a}{(1+e^{(-b(t-c))})} \tag{4}$$

Although the position and orientation are very significant variables, they have been discarded from the present regression analysis. It is not actually a value that can be introduced as an input to an equation and its presence would lead to underestimate the rest of the parameters. Further studies could analyse gradual misalignments and misorientations to add their effect.

Initially the more representative simulations have been fitted to the proposed function, obtaining the necessary *a*, *b* and *c* parameters on each, as summarised in Table 3. Subsequently, a multivariate linear regression analysis was conducted to establish the correlation between these parameters and the frequency considered and the diameter of the rebar embedded. As reported in Table 4, the covariates are not statistically significant for establishing a relationship with *a*. The relationships between frequency and *b* is positive, while between rebar diameter and *b* is negative. The higher the frequency, the higher the heating rate. However, the greater the rebar diameter the slower the heating takes place, since there is much more steel to heat. The opposite trend can be observed for *c*.

Checking standard residuals, no outliers are detected. The independence of observations is assessed with a Durbin-Watson test. Although the obtained value for *c* is rather high, applying a forward entry method shows that the second covariate is the reason. However, instead of dropping it, it is maintained in the model since it notably improves the model, substantially increasing R^2 from 0.796 to 0.979.

$$\begin{aligned} a &= 720 \\ b &= 0.07 + 0.002 \cdot f - 0.004 \cdot \Phi \\ c &= 27.516 - 0.527 \cdot f + 1.907 \cdot \Phi \end{aligned} \tag{5}$$

Considering Equation 5, other frequency and rebar combinations have been predicted. Due to the lack of statistical significance for *a*, an average value of 720 °C has

Table 4 Linear regression

Dependent variable	Covariate	R^2	Unstandardized coefficient	Significance p-value	Std. Residual		Durbin-Watson statistic
					Min.	Max.	
a	f	---	---	0.648	-1.732	0.895	2.310
	Φ		---	0.252			
	(intercept)		---				
b	f	0.980	0.002	0.002**	-1.457	1.457	2.102
	Φ		-0.004	0.028*			
	(intercept)		0.007				
c	f	0.979	-0.527	0.002**	-1.291	1.291	3.380
	Φ		1.097	0.014*			
	(intercept)		27.516				

*p-value<0.05; **p-value<0.01

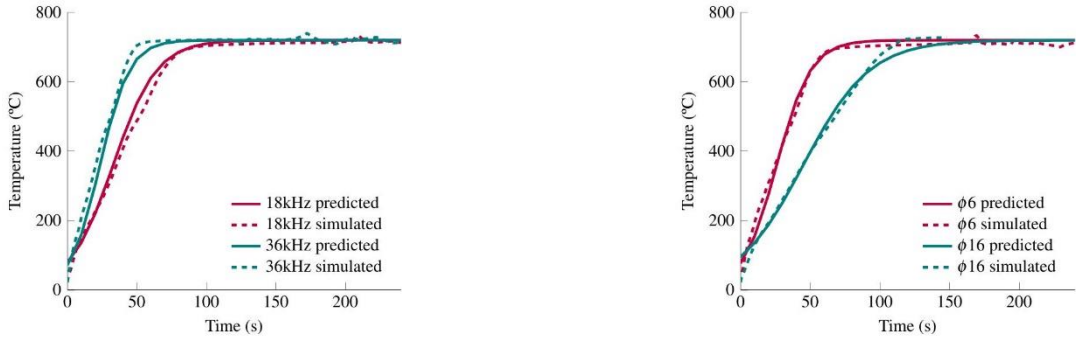

(a) Varying frequency (b) Varying diameter

Fig. 10 Predicted and simulated heating temperatures

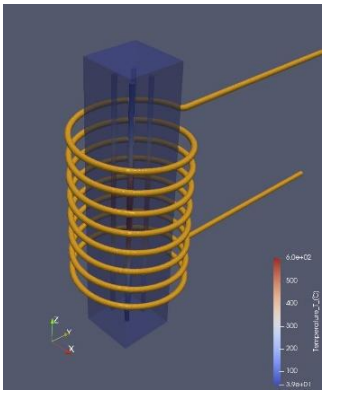

(a) Only vertical rebars

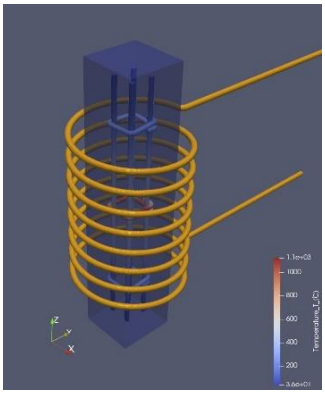

(b) Vertical rebars plus stirrups

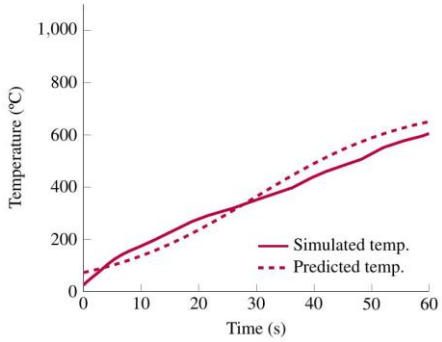

(c) Temperature increment on the vertical rebar without stirrups

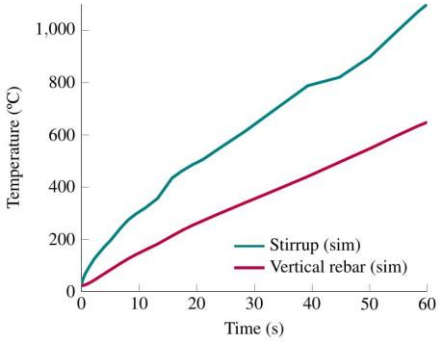

(d) Temperature increment with stirrups

Fig. 11 Test and simulations on columns

(a) Damage observed

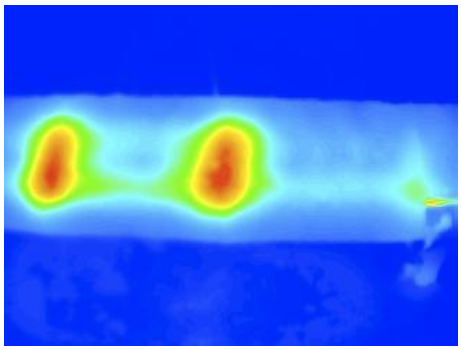

(b) Termographic image of the real test

Fig. 12 Test and simulations on columns

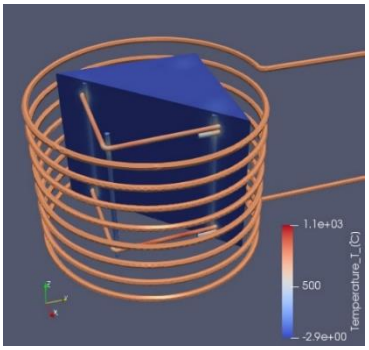

(a) Temperatures achieved on rebar and concrete

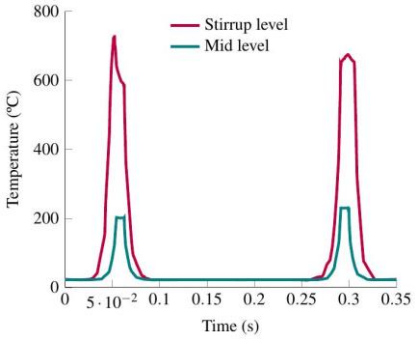

(b) Temperature along diagonal

Fig. 13 Temperature values on real size column

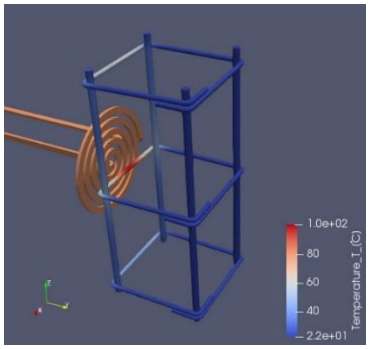

(a) Stirrup at the centre of the inductor

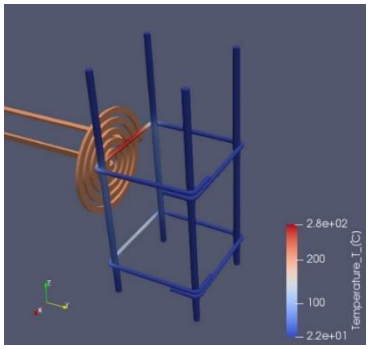

(b) Stirrup at a quarter of the stirrup

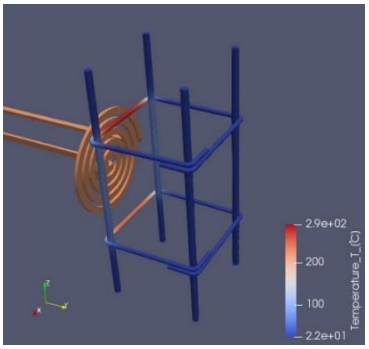

(c) Two stirrups at each edge of the inductor

Fig. 14 Spiral shape inductor

been considered. The other parameters adopt the coefficients shown in Table 4. Fig. 10 illustrates the adequacy of the predictions and the subsequent simulations.

4. Discussion

All the summarised findings heretofore lead to the feasibility of selectively damaging the cementitious matrices, such as concrete, in specific applications.

Corrosion phenomena on the reinforcement located in columns lead to, initially, cracking and, finally, the spalling of the concrete corners, providing a higher exposure of the steel to an aggressive environment. A preventive repair based on the passivation of the steel is essential in order to avoid an excessive mass loss that would require its substitution or the supplement of another rebar. Instead of employing pneumatic jackhammers to access the steel that produced common affections (mainly, noise and dust) and induced vibrations that could harm such a stiff structure, the local demolition can be accomplished efficiently surrounding the column with an inductor as depicted in Fig. 13.

The proposal is validated by testing a reduced scale column (see Fig. 12(b)) and comparing the results with an identical simulation (see Fig. 11(b)). Since the reinforcement does not involve a unique rebar but four, the consumed power increases accordingly. The power consumption corresponding to the steel quadruples the previous value, while the fraction of the inductor remains

constant.

Since the number of rebars increases substantially in these models, and hence so do the mesh elements due to the required viscous layers, the simulations where developed for 60 seconds, considering it time enough to achieve high temperatures.

The test, the simulation and the prediction equation developed in Subsection 3.8 for the scale column, lead to very similar values (See Fig. 11(c)), validating the procedure and foreseen a local damage and disgregation of the cementitious matrix and the steel reinforcement for the real case, in agreement with the phenomena described in Section 1. According to the scaled test and simulations, the vertical reinforcement can be heated up to 600 °C in barely 60 seconds, but in case stirrups are added to the model, as in the real test, this temperature improves slightly up to 650 °C. The reason for such unexpected behaviour lies in the presence of stirrups. Although previously it has been stated that horizontally located rebars do not heat notably, in case those rebars are a closed loop instead of a rectilinear piece, the induced horizontal currents (see Fig. 1) flow through a longer circuit and heat considerably faster, specially between vertical rebars, far above 1000 °C in the same time span, as can be observed in Fig. 11(d) and Fig. 12(b), providing a higher temperature to the vertical rebars due to conduction phenomena, where in contact with them. Fig. 12(a) clearly shows the damage caused, specially along the stirrups.

Considering a real size column (e.g., 350 mm-width) (see Fig. 13), the behaviour is consistent with the previous observations. The stirrups achieve their highest temperature in the straight section (above 1000 °C), clearly showing much higher temperatures on the rebars along a horizontal section including the stirrup, than those sections where there is not stirrup, as Fig. 13(b) illustrates. The discontinuity of the stirrups is the reason for the slight divergence in the maximum values observed. Moreover, in such a short time the temperature on the concrete only increases close to the reinforcement, protecting the core of the column from undesired damage in case of a superficial reparation is of interest.

In order to check whether this performance can be obtained with inductors that do not require to surround the column, several other simulations where performed with a spiral shape. As shown in Fig. 14, the relative position of the inductor and the stirrup play a key role but, by far, the temperatures are not as high as with the helix shape inductor. This kind of inductor do not provide enough continuity in the magnetic field created along the sirrup, to induce a remarkable current.

Apart from what has already been observed during the real test for the scaled columns, and since there was not availability of a greater inductor such as the one considered in the simulation (see Fig. 13(a)), a finite element model was build and analysed taking into account common steel reinforcement (S500) and concrete (C25/30). The cracking behaviour of the concrete was assessed according to Eq. 6, obtaining an approximate value of 2.5 MPa. Besides, and from a more realistic approach, the concrete and rebars were subjected to a preload of 7 and 40 MPa, respectively, that simulated a serviceability state.

$$f_{ct,m} = 0{,}3 \cdot \sqrt[3]{f_{ck}{}^2} \tag{6}$$

Fig. 15(a) shows the cracking pattern developed in the concrete column subjected to the heating simulation. The combination of vertical cracks, both in the plane among stirrups (violet) and containing the vertical rebars (yellow), and horizontal ones, from the stirrups to the surface (green), would allow to remove the concrete cover over the steel without incurring in damages on the core of the column. The thermal shock and elongation of the steel would cause cracks that would delimit blocks with sizes equal to stirrup and vertical rebar distances and with the cover distance as thickness.

Although the simulation explains the development of three different types of cracks, the real test mainly shows the horizontal cracks from the stirrups to the surface (see Fig. 12(a)). The lack of the mentioned preload in the specimen allows the formation of those cracks in the first place since the stirrups achieve higher temperatures. In a real case, the load born by the column would restrain the development of such crack and, therefore, retain the steam generated by the heating of the moisture trapped in the concrete, favouring the evolution of the other crack types.

5. Conclusions

The present study tests and simulates the heating process of cementitious matrices with embedded steel reinforcements. Different values are adopted for the parameters involved, such as, the position and diameter of the rebar, the frequency of the magnetic field, the thermal conductivity and the specific heat capacity of the matrix and the convection and radiation on the surface of the specimen. The results prove the suitability of induction heating to cause a thermal shock between the steel reinforcement and the concrete almost immediately (<90 s).

- High temperatures (above 700 °C) are achieved in less than 90 s.
- Temperature is high enough to damage the bonding of the reinforcement and degrade the main matrix components, decomposing calcium silicate hydrate (CSH) and portlandite.
- The cracking caused by the thermal shock due to the sudden heating of the steel, is intensified by the steam pressure provoked by the evaporation of the moisture contained in the capillary pores of the matrix.
- Frequency and position are the most influential parameters.
- Setting the frequency is crucial due to its impact in the skin depth. Higher frequencies focus the heating process in lower thicknesses, consuming all the power in a smaller volume and therefore, increasing the intensity of the joule heating process. The heating rate increases up to 300% when the frequency escalates from 12 kHz to 48 kHz.
- As a drawback, induction equipment with higher working frequencies are more expensive. Therefore,

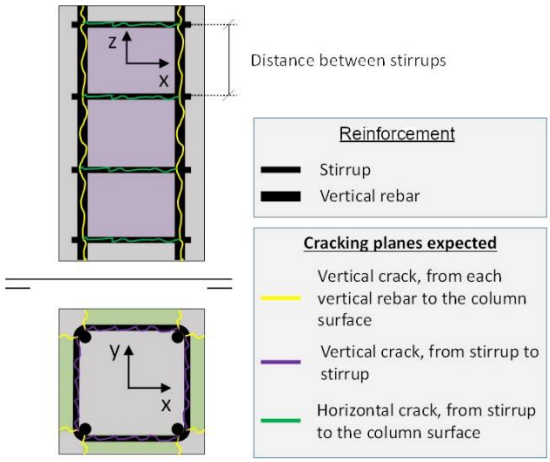

(a) Cracking scheme

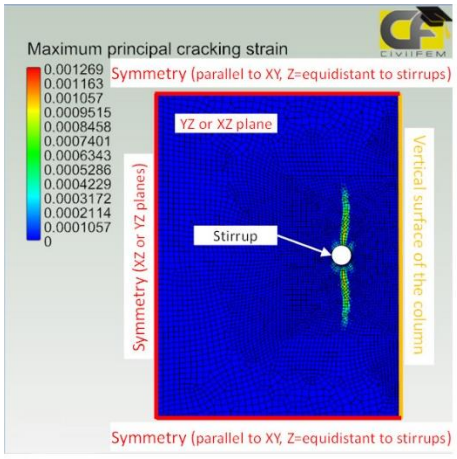

(a) Vertical section

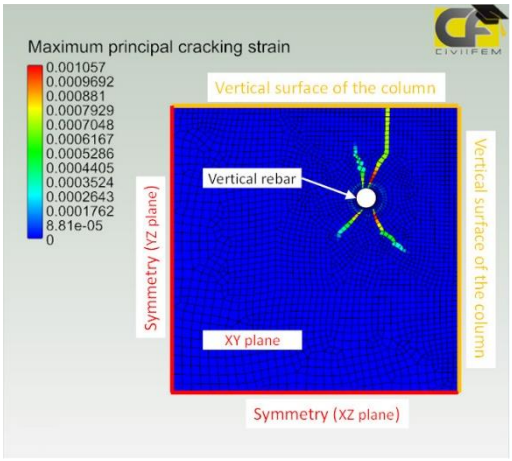

(b) Horizontal section

Fig. 15 Finite element cracking model

there is a high interest in simulations that allow to design accurately any geometry saving the cost of real tests at diverse frequencies.

• The position and orientation of the reinforcement is of paramount importance since its proximity and alignment with the magnetic field leads to different performances. Orientations aligned and misaligned with the magnetic field present maximum temperatures that differ up to 250%.

• The increase of the thermal conductivity of the cementitious matrix, allows a higher heat transfer between steel and mortar reducing the heating ratio of the reinforcement during the initial stage. The effect in the exterior surface is limited.

• Specific heat capacity shows a quite opposite behaviour affecting more the surface temperature of the mortar rather than the temperature in the steel.

• Convection and emissivity are factors that have a low impact in the temperature achieved. The low surface area/volume ratio and the surface temperatures are not enough to produce noticeable effects.

• The prediction model properly fits (R^2=0.979) the heating ratio saving costs of further tests.

• The horizontal stirrups of a column can play a key role, achieving higher temperatures (above 1000 °C) in case they are composed of closed, preferably welded, rebars.

Future research could contemplate steel fibres as reinforcement, consequently restraining the matrix cracking and allowing a higher vapour pressure within the specimen that will lead to, finally, disaggregate the cementititous matrix from the steel. Likewise, the mixing of blowing agents as an additional aggregate that would activate at high temperatures expelling higher amounts of water vapour or CO_2, could also expedite the rupture.

Further studies, due to the results obtained for the scaled columns, could consider a new approach where the target of the induction heating could be the stirrups and similar rebars designed as closed loops and located according to the induced current flow. This would expedite the expected damage and become feasible its implementation on various structural, reinforcement or demolition projects for applications such as buildings, railway infrastructures, etc. A similar parametric study could lead to establish prediction models fitted for different applications and geometries.

Acknowledgments

The authors wish to acknowledge the financial funding

of the European Horizon 2020 Joint Technology Initiative Shift2Rail, through contracts no. 826255 & 101012456 (IN2TRACK2 & IN2TRACK3), the Basque Government through Elkartek 2019 ref. KK-2019/00023, PID2021-124203OB-I00 and the participation of IT1764-22 and IT1619-22 (SAREN) research groups and RTI2018-097079-B-C31 funded by MICIU/AEI/10.13039/501100011033 and by "ERDF A way of making Europe", by the "European Union". Finally, the authors acknowledge the support from CENOS and CivilFEM through its induction simulation and finite element software, respectively, and IZO-SGI SGIker of UPV/EHU for the technical assistance.

References

Ahn, C.H., Lee, J., Kim, D.J. and Shin, H.O. (2021), "Development of a novel concrete curing method using induction heating system", *Appl. Sci.*, **11**(1), 236. https://doi.org/10.3390/app11010236.

Akbarnezhad, A. and Ong, K. (2011), "Thermal stress and pore pressure development in microwave heated concrete", *Comput. Concrete*, **8**(4), 425-443. https://doi.org/10.12989/cac.2011.8.4.425.

Borinaga-Treviño, R., Orbe, A., Cuadrado, J., Crespo, I. and Norambuena-Contreras, J. (2019), "Microwave and induction heating on fibre-reinforced cementitious materials for the demolition of structures", *AMPERE 2019 - 17th International Conference on Microwave and High Frequency Heating*, Valencia, Spain, September.

Canbaz, M., Dakman, H., Arslan, B. and Büyüksungur, A. (2019), "The effect of high-temperature on foamed concrete", *Comput. Concrete*, **24**(1), 1-6. https://doi.org/10.12989/cac.2019.24.1.001.

Davies, E. (1990), *Conduction and Induction Heating*, The Institution of Engineering and Technology (IET), London, UK.

De Wolf, C., Cordella, M., Dodd, N., Byers, B. and Donatello, S. (2023), "Whole life cycle environmental impact assessment of buildings: Developing software tool and database support for the EU framework Level(s)", *Resour. Conserv. Recycl.*, **188**, 106642. https://doi.org/10.1016/j.resconrec.2022.106642.

Di Maria, A., Eyckmans, J. and Van Acker, K. (2020), "26 - Use of LCA and LCC to help decision-making between downcycling versus recycling of construction and demolition waste", *Advances in Construction and Demolition Waste Recycling*, Woodhead Publishing, Duxford, UK.

European Commission (2018), Consolidated Text: Directive 2008/98/EC of the European Parliament and of the Council of 19 November 2008 on Waste and Repealing Certain DIRECTIVES (Text with EEA relevance), The European Parliament and the Council of the European Union, Strasbourg, France.

European Environment Agency (2020), "Resource efficiency and the circular economy in Europe 2019 - Even more from less - An overview of the policies, approaches and targets of 32 European countries", EEA Report/No 26/2019; European Environment Agency, Copenhagen, Denmark.

Ferrara, L., Faifer, M. and Toscani, S. (2012), "A magnetic method for non destructive monitoring of fiber dispersion and orientation in steel fiber reinforced cementitious composites-Part 1: Method calibration", *Mater. Struct.*, **45**(4), 575-589. https://doi.org/10.1617/s11527-011-9793-y.

Fufa, S.M., Fjellheim, K., Venås, C., Vevatne, J.T., Kummen, T.M. and Henke, L. (2023), "Waste free construction siteA buzzword, nice to have or more", *Resour. Conserv. Recycl. Adv.*, **18**, 200149. https://doi.org/10.1016/j.rcradv.2023.200149.

García, A., Norambuena-Contreras, J. and Partl, M.N. (2013), "Experimental evaluation of dense asphalt concrete properties for induction heating purposes", *Constr. Build. Mater.*, **46**, 48-54. https://doi.org/10.1016/j.conbuildmat.2013.04.030.

Hondroyiannis, G., Sardianou, E., Nikou, V., Evangelinos, K. and Nikolaou, I. (2024), "Circular economy and macroeconomic performance: Evidence across 28 European countries", *Ecol. Econom.*, **215**, 108002. https://doi.org/10.1016/j.ecolecon.2023.108002.

Jankowski, T.A., Pawley, N.H., Gonzales, L.M., Ross, C.A. and Jurney, J.D. (2016), "Approximate analytical solution for induction heating of solid cylinders", *Appl. Math. Model.*, **40**(4), 2770-2782.

Kabirifar, K., Mojtahedi, M., Wang, C. and Tam, V.W. (2020), "Construction and demolition waste management contributing factors coupled with reduce, reuse, and recycle strategies for effective waste management: A review", *J. Clean. Prod.*, **263**, 121265. https://doi.org/10.1016/j.jclepro.2020.121265.

Kennedy, M.W., Akhtar, S., Bakken, J.A. and Aune, R.E. (2012), "Analytical and FEM modeling of aluminum billet induction heating with experimental verification", *Light Metals*, Springer International Publishing, Orlando, FL, USA.

Kim, G.J. and Kwak, H.G. (2017), "Depth-dependent evaluation of residual material properties of fire-damaged concrete", *Comput. Concrete*, **20**(4), 503-509. https://doi.org/10.12989/cac.2017.20.4.503.

Kobayashi, K. and Banthia, N. (2011), "Corrosion detection in reinforced concrete using induction heating and infrared thermography", *J. Civil Struct. Health Monit.*, **1**, 25-35. https://doi.org/10.1007/s13349-010-0002-4.

Lei, H., Li, L., Yang, W., Bian, Y. and Li, C.Q. (2021), "An analytical review on application of life cycle assessment in circular economy for built environment", *J. Build. Eng.*, **44**, 103374. https://doi.org/10.1016/j.jobe.2021.103374.

Li, L., Zhang, H., Dong, J., Zhang, H., Jia, P., Wang, Q. and Liu, Y. (2019), "Recovery of mortar-aggregate interface of fire-damaged concrete after post-fire curing", *Comput. Concrete*, **24**(3), 249-258. https://doi.org/10.12989/cac.2019.24.3.249.

Liang, J.F., Wang, E., Zhou, X. and Le, Q.L. (2018), "Influence of high temperature on mechanical properties of concrete containing recycled fine aggregate", *Comput. Concrete*, **21**(1), 87-94. https://doi.org/10.12989/cac.2018.21.1.087.

Liang, J.F., Yang, Z.P., Yi, P.H. and Wang, J.B. (2017), "Stress-strain relationship for recycled aggregate concrete after exposure to elevated temperatures", *Comput. Concrete*, **19**(6), 609-615. https://doi.org/10.12989/cac.2017.19.6.609.

Lim, M. and Kim, H. (2017), "Economic feasibility of the induction heating method for dismantling structures: Analysis of direct construction cost based on required demolition equipment", *Int. J. Appl. Eng. Res.*, **12**(23), 13416-13423.

Lim, M.K. and Lee, C. (2021), "A study on the heat and stress evaluation of reinforced concrete through high-frequency induction heating system using finite element techniques", *Sustainab.*, **13**(11), 6061. https://doi.org/10.3390/su13116061.

Lim, M.K. and Lee, C. (2021), "Evaluation of heating technique of deformed reinforcement using high-frequency induction heating system", *Appl. Sci.*, **11**(11), 4947. https://doi.org/10.3390/app11114947.

Lim, M.K. and Lee, C. (2021), "Evaluation of weakening characteristics of reinforced concrete using high-frequency induction heating method", *Appl. Sci.*, **11**(12), 5402. https://doi.org/10.3390/app11125402.

Lim, M.K., Park, J.H. and Wook, H.J. (2017), "Development of a method to make existing reinforced concrete structures fragile, using the principle of Induction Heating", *Int. J. Appl. Eng.*

Res., **12**(23), 13015-13022.
Liu, L., Zheng, D., Zhou, J., He, J., Xin, J. and Cao, Y. (2018), "Corrosion detection of bridge reinforced concrete with induction heating and infrared thermography", *Int. J. Robot. Automat.*, **33**(4), 379-385. http://doi.org/10.2316/Journal.206.2018.4.206-5085.
Luozzo, N.D., Fontana, M. and Arcondo, B. (2012), "Modelling of induction heating of carbon steel tubes: Mathematical analysis, numerical simulation and validation", *J. Alloys Comp.*, **536**(1), S564-S568. https://doi.org/10.1016/j.jallcom.2011.12.084.
Luu, N.C., Nguyen, L.H., Tran, T.V.N., Isobe, Y., Kawasaki, M. and Kawamoto, K. (2021), "Construction and demolition waste illegal dumping: Environmental, social and economic impacts assessment for a growing city", *Japanese Geotech. Soc.*, **9**, 148-155. https://doi.org/10.3208/jgssp.v09.cpeg133.
Lynch, N. (2022), "Unbuilding the city: Deconstruction and the circular economy in Vancouver", *Environ. Plan. A: Econ. Sp.*, **54**(8), 1586-1603, https://doi.org/10.1177/0308518X221116891.
Menard, Y., Bru, K., Touze, S., Lemoign, A., Poirier, J., Ruffie, G., Bonnaudin, F. and Von Der Weid, F. (2013), "Innovative process routes for a high-quality concrete recycling", *Waste Manag.*, **33**(6), 1561-1565. https://doi.org/10.1016/j.wasman.2013.02.006.
Moncaster, A. and Symons, K. (2013), "A method and tool for 'cradle to grave' embodied carbon and energy impacts of UK buildings in compliance with the new TC350 standards", *Energy Build.*, **66**, 514-523. https://doi.org/10.1016/j.enbuild.2013.07.046.
Nemkov, V. and Goldstein, R. (2017), "Striation effect in induction heating: Myths and reality", *Int. J. Comput. Math. Electr. Electron. Eng.*, **36**(2), 504-517. https://doi.org/10.1108/COMPEL-05-2016-0189.
Norambuena-Contreras, J., Serpell, R., Valdés Vidal, G., González, A. and Schlangen, E. (2016), "Effect of fibres addition on the physical and mechanical properties of asphalt mixtures with crack-healing purposes by microwave radiation", *Constr. Build. Mater.*, **127**, 369-382. https://doi.org/10.1016/j.conbuildmat.2016.10.005.
Ong, K. and Akbarnezhad, A. (2015), *Microwave-Assisted Concrete Technology: Production, Demolition and Recycling*, CRC Press, Taylor & Francis Group, Boca Raton, FL, USA.
Orbe, A., Rojí, E., Losada, R. and Cuadrado, J. (2014), "Calibration patterns for predicting residual strengths of steel fibre reinforced concrete (SFRC)", *Compos. Part B: Eng.*, **58**, 408-417. https://doi.org/10.1016/j.compositesb.2013.10.086.
Ozbolt, J., Periŝkić, G., Reinhardt, H.W. and Eligehausen, R. (2008), "Numerical analysis of spalling of concrete cover at high temperature", *Comput. Concrete*, **5**(4), 279-293. https://doi.org/10.12989/cac.2008.5.4.279.
Qabaja, M. and Tenekeci, G. (2023), "Nexus between construction sector and economic indicators for Turkey and European Union evidenced by panel data analysis", *Eng. Constr. Arch. Manag.*, **30**(5), 1978-2007. https://doi.org/10.1108/ECAM-10-2021-0927.
RILEM Technical Committee 227 (2019a), *State-of-the-Art Report of the RILEM Technical Committee 227-HPB, Modelling of Concrete Behaviour at High Temperature*, Springer, Cham, Switzerland.
RILEM Technical Committee 227 (2019b), *State-of-the-Art Report of the RILEM Technical Committee 227-HPB, Physical Properties and Behaviour of High-Performance Concrete at High Temperature*, Springer, Cham, Switzerland.
Sannikov, D.V., Kolevatov, A.S., Vavilov, V.P. and Kuimova, M.V. (2018), "Evaluating the quality of reinforced concrete electric railway poles by thermal nondestructive testing", *Appl. Sci.*, **8**(2), 222. https://doi.org/10.3390/app8020222.
Silvestre, J., de Brito, J. and Pinheiro, M. (2014), "Environmental impacts and benefits of the end-of-life of building materials - calculation rules, results and contribution to a "cradle to cradle" life cycle", *J. Clean. Prod.*, **66**, 37-45. https://doi.org/10.1016/j.jclepro.2013.10.028.
Silvestre, J.D., de Brito, J. and Pinheiro, M.D. (2013), "From the new European Standards to an environmental, energy and economic assessment of building assemblies from cradle-to-cradle (3E-C2C)", *Energy Build.*, **64**, 199-208. https://doi.org/10.1016/j.enbuild.2013.05.001.
Torrents, J., Blanco, A., Pujadas, P., Aguado, A., Juan-García, P. and Sánchez-Moragues, M. (2012), "Inductive method for assessing the amount and orientation of steel fibers in concrete", *Mater. Struct.*, **45**, 1577-1592. https://doi.org/10.1617/s11527-012-9858-6.
Wang, B., Pan, J., Fang, R. and Wang, Q. (2020), "Damage model of concrete subjected to coupling chemical attacks and freeze-thaw cycles in saline soil area", *Constr. Build. Mater.*, **242**, 118205. https://doi.org/10.1016/j.conbuildmat.2020.118205.
Yan, L.L., Liang, J.F. and gang Zhao, Y. (2019), "Effect of high temperature on the bond performance between steel bars and recycled aggregate concrete", *Comput. Concrete*, **23**(3), 155-160. https://doi.org/10.12989/cac.2019.23.3.155.
Zhang, H., Zhou, J., Zhao, R., Liao, L., Yang, M. and Xia, R. (2017), "Experimental study on detection of rebar corrosion in concrete based on metal magnetic memory", *Int. J. Robot. Automat.*, **32**(5), 530-537. https://doi.org/10.2316/journal.206.2017.5.206-5082.
Zhang, M., Liu, X. and Kong, L. (2023), "Evaluation of carbon and economic benefits of producing recycled aggregates from construction and demolition waste", *J. Clean. Prod.*, **425**, 138946. https://doi.org/10.1016/j.jclepro.2023.138946.

CC